RESEARCH Open Access

White adipose tissue undergoes pathological dysfunction in the TDP-43^{A315T} mouse model of amyotrophic lateral sclerosis (ALS)



Cristina Benito-Casado¹, Esther Durán-Mateos², Águeda Ferrer-Donato¹, Gemma Barroso García³, Raúl Domínguez-Rubio^{4,5}, Mónica Povedano^{4,5} and Carmen M. Fernandez-Martos^{1,6*}

Abstract

White adipose tissue (WAT) has a crucial role in maintaining systemic energy homeostasis. Numerous biological pathway studies have highlighted the importance of adipokines in regulating metabolic pathways and contributing to metabolic dysfunction in animal models and patients with ALS. Despite these associations, the specific molecular mechanisms remain poorly understood. Moreover, the direct contribution of WAT to the energy metabolism abnormalities observed in ALS has yet to be clearly defined. The current study sought to identify perturbances in WAT, main source of leptin, during the clinical course of the disease in TDP-43^{A315T} mice using histological, proteomic, and molecular biological techniques. We present the first evidence of a significant histological alteration in WAT prior to the symptomatic stage of the disease in TDP-43^{A315T} mice, providing novel insights into pathological features earlier in the onset of symptoms, and showing WAT as a target organ for ALS. In human ALS cases, we found that circulating leptin levels at the time of diagnosis were lower in the plasma of men with ALS who were overweight or obese and had rapidly progressive ALS, emphasizing the importance of considering sex-specific approaches when analysing adipokines essential for body weight control.

Keywords Amyotrophic lateral sclerosis (ALS), TAR DNA binding protein (TDP-43), White adipose tissue (WAT), Sporadic ALS

*Correspondence:

Carmen M. Fernandez-Martos

Carmen.fernandezmartos@ceu.es

- ¹ Department of Health and Pharmaceutical Sciences, School of Pharmacy, Universidad CEU-San Pablo, Urbanización Monteprincipe, Boadilla del Monte, 28660 Madrid, Spain
- ² Department of Basic Medical Sciences, School of Medicine, Universidad CEU-San Pablo, Madrid, Spain
- ³ SESCAM, SAI-Proteómica, Hospital Nacional de Parapléjicos, SAI-HNP-IDISCAM, Toledo, Spain
- ⁴ Functional Motorneuron Unit (UFMN), Service of Neurology, Bellvitge University Hospital, Hospitalet de Llobregat, Spain
- ⁵ Instituto de investigación biomédica de Bellvitge (IDIBELL), Hospitalet de Llobregat, Spain
- ⁶ Wicking Dementia Research and Education Centre, University of Tasmania, Tasmania, Australia

Introduction

Amyotrophic lateral sclerosis (ALS) is the third most common neurodegenerative disease worldwide characterized by the selective loss of motor neurons both in the brain and spinal cord [38], leading to paralysis and respiratory failure. ALS is often rapidly progressive, incurable, and fatal. Over 60% of patients die within 3–5 years after diagnosis [8]. Although much effort has been made in the past two decades to understand the complexity and heterogeneity of ALS, the development of effective therapies remains elusive due to several challenges. One major obstacle is the limited understanding of the underlying mechanisms driving ALS disease.



© The Author(s) 2025. **Open Access** This article is licensed under a Creative Commons Attribution-NonCommercial-NoDerivatives 4.0 International License, which permits any non-commercial use, sharing, distribution and reproduction in any medium or format, as long as you give appropriate credit to the original author(s) and the source, provide a link to the Creative Commons licence, and indicate if you modified the licensed material. You do not have permission under this licence to share adapted material derived from this article or parts of it. The images or other third party material in this article are included in the article's Creative Commons licence, unless indicated otherwise in a credit line to the material. If material is not included in the article's Creative Commons licence and your intended use is not permitted by statutory regulation or exceeds the permitted use, you will need to obtain permission directly from the copyright holder. To view a copy of this licence, visit http://creativecommons.org/licenses/by-nc-nd/4.0/.

Identifying the mechanisms involved in maintaining energy homeostasis in ALS can help to elucidate the growing evidence supporting a strong metabolic component in ALS. Indeed, rapid weight loss is associated with worse disease outcomes in ALS [22], and fat mass loss correlates with faster disease progression [25]. Conversely, higher initial body mass index (BMI) and obesity [21], type 2 diabetes mellitus [23], and patients with higher triglyceride and cholesterol levels [11] have been associated with longer survival in ALS, indicating fat content and lipid metabolism are important prognostic factors in ALS disease. However, despite these correlations, the underlying mechanisms driving these metabolic derangements remain unclear. Adipose tissue is an endocrine organ and constitute the major lipid store in mammals [24]. Two main types of anatomically and physiologically different adipose tissue are present in adults: WAT, which is mainly an energy store [29]; and the brown adipose tissue (BAT), with specialized functions in heat production (thermogenesis) [26]. Moreover, as an endocrine organ, adipose tissue secretes a variety of soluble mediators, with a critical role in the physiological regulation of the metabolism acting on the hypothalamus, a key integrative brain area that regulates neuronal and metabolic circuits involved in energy intake regulation [17]. While dysfunctions in the hypothalamus have only recently been described [37], studies have shown this brain structure is atrophied in ALS [43], even in premorbid stages, and correlates with BMI [18]. Altered eating behaviour have been reported in patients with ALS and frontotemporal dementia (FTD) [1]. Indeed, we and others demonstrated increased mRNA expression levels of agouti-related peptide (AgRP), while levels of its antagonist pro-opiomelanocortin (POMC) were decreased in the hypothalamus in TDP-43^{A315T} mice [16] and mutant SOD1^{G86R} mice [44], demonstrating of a hypothalamic involvement in ALS. Indeed, there are several adipokines involved in metabolism and regulation of food intake which act within the brain, specifically in the brainstem and hypothalamus, including, but not limited to, leptin, which is primarily produced by WAT in proportion to fat stores [35]. Nevertheless, although clinical evidence suggests that the distribution and content of adipose tissue, and subsequently leptin levels, are significantly altered in ALS and have been correlated with functional status and survival in ALS [16, 33, 34], it is currently unclear whether metabolic changes in ALS are driven by the adipose tissue dysfunction, or whether hypothalamic neuronal dysfunction may contribute to disease processes in ALS.

Notably, metabolic changes are also observed in FTD, which exists on a continuous clinical spectrum with ALS [7]. Indeed, although the clinical manifestations of ALS

and FTD differ [7], altered peripheral levels of leptin have been found in patients with FTD [2], while there is also limited information on the mechanism underlying the association between adiposity and brain metabolism. Furthermore, we have determined complex alterations in metabolic hormones, including leptin, in pathologyrich regions of post-mortem human ALS and FTD tissues [4], which is in agreement with our previous results in TDP-43^{A315T} mice showing that alterations to TDP-43 are linked to reduced circulating levels of leptin and the dysfunction of its signalling pathways at the central nervous system (CNS) [16]. These data are of interest because studies have suggested that higher leptin levels are critical for survival in ALS disease, as leptin levels have been found to be lower in sporadic ALS patients with rapidly progressing disease [34], which is in agreement with our previous studies in TDP-43^{A315T} mice showing the potential benefit of leptin therapy against ALS [15]. Thus, it will be important to study the possible alterations occurring in WAT, which could perturb peripheral to CNS communication, leading to skeletal muscle degeneration in ALS.

Here we aimed to better understand whether the WAT plays a critical role in the pathophysiology of ALS, as most ALS patients have hypermetabolism [12] and weight loss [9] prior to the onset of motor symptoms. In this context, considering the potential remodelling of WAT and its important role in whole-body homeostasis, we comprehensively characterized changes in WAT at different stages of the disease (asymptomatic, onset and end-stage) in TDP-43A315T mice compared to gender and age-matched wild-type (WT) littermates, using histology, proteomics method, and molecular biology techniques. In addition, as epidemiological evidence suggests, alterations in leptin levels are associated with changes in disease progression and survival in ALS. Plasma samples of patients with ALS were used to assess sex and BMI differences in leptin concentrations at the time of diagnoses, to determine if leptin may serve as prognostic biomarker in ALS. Exploring these links may help to better understand the mechanisms underlying the relationship between adiposity and disruption in leptin levels in ALS, because, although BMI is the most used measure of global adiposity, it does not represent adiposity in terms of regional fat distribution, which differs between sexes, races and ages.

Materials and methods

Experimental animals

Two cohorts of sex and age-matched WT non-transgenic littermates (C57Bl/6) and TDP- 43^{A315T} mice [46] (n=60/genotype) were used in this study to conduct histology (n=30/genotype), proteomic and molecular biology techniques (n=30/genotype). In both cases, the ALS-like disease was divided into three stages (n=5/stage):

asymptomatic, onset (defined as the last day of individual peak body weight before a gradual loss occurs) and the end-stage of disease (defined as when weight is 20% below the initial weight on three consecutive days), which is typically reached 2–4 weeks after symptom onset. To avoid the ambiguity associated with reported sex-related differences in mean survival time of this mouse model of ALS [20, 46], only male mice were used. Animals were euthanized independently on each stage of disease. Animals expressing the human TDP-43 (hTDP-43) transgene were confirmed via PCR according to the distributor's protocol.

To monitor disease onset and progression, all mice were weighed and assessed three times per week until the disease onset-stage, after which they were checked daily in the morning until the disease end-stage. The maintenance and use of mice and all experimental procedures were approved by the Animal Ethics Committee of the Hospital Nacional de Parapléjicos, Toledo (Spain) (Approval No 26/OH 2018) in accordance with the Spanish Guidelines for the Care and Use of Animals for Scientific Purposes. All analyses were conducted by personnel blinded to the animal genotype.

Perfusion and tissue collection

Animals were terminally anesthetized with sodium pentobarbitone (140 mg/kg, intraperitoneally) and transcardially perfused with 0.01 M PBS (pH 7.4). For immunohistochemistry, subcutaneous WAT (scWAT) and perigonadal WAT (pgWAT) were immediately dissected, rinsed in cold phosphate buffered saline (PBS), postfixed 70% ethanol, and stored at 4°C until paraffin embedding using an Automatic Tissue Processor (ATP 1000, Histo-line, Italy), for further use. For molecular biology experiments, scWAT and pgWAT tissues of each animal were split into two fractions and processed independently, for real time qPCR and Western blot analysis, or proteomics methods. Samples were immediately frozen on dry ice and stored at –80 °C for later analysis.

Immunohistochemistry (IHC)

Paraffin-embedded Sects. (4 µm thick) of scWAT and pgWAT were deparaffinized in xylene and rehydrated through descending grades of ethanol (100%, 95%, 90%, 80% and 70%) to water. Sections were stained with hematoxylin and eosin (H&E), dehydrated through ascending grades of ethanol (75%, 95%, and 100%), cleared in xylene and finally mounted in dibutyl phthalate xylene (DPX). For analysis, digital photomicrographs of the entire scWAT and pgWAT tissue Sects. (20x; Leica CTR 6000, Leica, Mannheim, Germany) were used to quantify the histochemical staining in 10 random fields for each sample different regions to assess the regional heterogeneity

in tissue samples. The regions were outlined using ImageJ software (Rasband, W.S., ImageJ, U. S. National Institutes of Health, Bethesda, Maryland, USA, https://imagej.net/ij/, 1997–2018). All slides were analysed using the same morphologic criteria for the quantification of crownlike structures (CLSs), defined by the clustering of macrophages (identified by each morphology) to surround a dying adipocyte, as a sign of adipose-tissue inflammation. This criterion was: presence of a ring of mononuclear cells surrounding an adipocyte vacuole. In addition, the number of blood vessels (BV) was also determined to assess vascularity as an index of angiogenesis.

Finally, by semiquantitative methods we determined inflammatory markers such as mononuclear infiltrate and fibrosis, and necrosis markers such as adipocyte normal membrane shape and tissue integrity. Semiquantitative scores were assigned by an observer based on predefined morphologic criteria: 1 (<25%), 2 (25-50%), 3 (51-75%), and 4 (>75%). Measure 10 fields at $10\times$ in simple scWAT and pgWAT tissues (n=60). All analyses were conducted by personnel blinded to animal genotype.

Total protein preparation and mass spectrometry analysis Sample preparation for library generation

Proteins were separated on precast gel, 4-20% Mini-PROTEAN TGX (BioRad) and visualized by Coomassie staining. The entire gel lane was manually cut into 8 sections and subjected to in-gel tryptic digestion. The digestion was performed according to Schevchenko et al. [40] with minor modifications: gel slices were incubated with 10 mM dithiothreitol (DTT; Sigma Aldrich) in 50 mM ammonium bicarbonate (99% purity; Scharlau) for 60 min at 37°C and after reduction, alkylation with 55 mM iodoacetamide (IAA; Sigma Aldrich) in 50 mM ammonium bicarbonate was carried out for 20 min at RT. Gel plugs were washed with 50 mM ammonium bicarbonate in 50% methanol (gradient, HPLC grade, Scharlau), rinsed in acetonitrile (ACN, gradient, HPLC grade, Scharlau) and dried in a Speedvac. Dry gel pieces were then embedded in sequencing grade modified porcine trypsin (Promega, Madison, WI, USA) at a final concentration of 12.5 ng/µL in 20 mM ammonium bicarbonate. After digestion at 37 °C overnight, peptides were extracted with 60% acetonitrile in 0.5% formic acid (FA, 99.5% purity; Sigma Aldrich) and the samples were resuspended in 10µL [98% water with 2% formic acid and 2% ACN].

Sample preparation for SWATH analysis

Samples lysates were digested using Single-pot solidphase-enhanced sample preparation (SP3) according to the protocol of Hughes et al. The lysates were reduced and alkylated using DTT and IAA, respectively. After reduction and alkylation, 6 μL of the prepared bead mix was added to the lysate and made up to 30 μL using H2O. Afterward, EtOH was added to a final concentration of 70% (v / v) and the samples were left stirring at 1000 rpm and room temperature for 20 min. Subsequently, the beads were immobilized by incubation on a magnetic rack for 2 min. The supernatant was recovered in a new vial, and the entire procedure was repeated. The pellet was rinsed with 80% (v / v) EtOH in water several times. The beads were resuspended in 300 μ l of 100 mM NH4HCO3 supplemented with trypsin in an enzyme to protein ratio of 1:25 (w / w). After digestion overnight at 37 °C and 1000 rpm, the samples are centrifuged at 20,000 g, the supernatant is collected and acidified using 2% FA.

LCMSMS Analysis for library, DDA and SWATH

In order to build the spectral library, the peptides extract were analysed by a shotgun approach by nanoLC-MS/ MS. Samples were pooled and 3 µg was separated into a Ekspert[™] nanoLC425 (Eksigent, Dublin, CA, USA) using a C18 column (ChromXPC18, 3 µm, 120 Å 0.075 × 150 mm, Eksigent) at a flow rate of 300nL/min in combination with a precolumn (NanoLC Trap ChromXP C18, 3 μ m 120 Å, Eksigent) at a flow rate of 5μ L/min. The buffers being used were: A = 0.1%FA 2%ACN and B = 98%ACN in water with 0.1% FA. Peptide were desalted for 3 min with 0.1%FA/2% ACN on the precolumn, followed by a separation for 85 min using gradient from 5 to 30% solvent B, 30–95% for 0.1 min, and finally 95%B for 5 min. Column was then regenerated with 5%B for 10 additional minutes. Peptides eluted were directly injected into a hybrid quadrupole-TOF mass spectrometer TripleTOF® 6600+(Sciex, Redwood City, CA, USA). Sample was ionized in a source type Optiflow < 1µL Nano applying 3.0 kV to the spray emitter at 200°C. Analysis was carried out in a data-dependent positive ion mode (DDA). Survey MS1 scans were acquired 350-1400 m/z for 250 ms. The TripleTOF was operated in SWATH mode, in which a 50 ms TOF MS scan from 350 to 1400 m/z was performed, followed by 50 ms product ion scans from 100 to 1500 m/z on the 70 variable windows from 350 to 1400 Da (2.20 s/cycle). The individual SWATH injections were randomized.

Protein data analysis

Peptide and protein identifications were performed using ProteinPilot[™] Software V 5.0 (Sciex) and the Paragon algorithm [41]. Each MS/MS spectrum was searched against the uniprot-proteome MusMusculus 2021 04 database, with the fixed modification of carbamidomethyl-labelled cysteine parameter enabled. Other parameters such as the tryptic cleavage specificity, the precursor ion mass accuracy and the fragment ion mass accuracy, are TripleTOF® 6600plus built in functions of the ProteinPilot software. SWATH Acquisition Micro-App v.2.0 was used for building a peptide spectral library containing the peptide identified in the database search with confidence score above 95%. SWATH Acquisition MicroApp was used for extracting the ion chromatogram traces from the SWATH raw files and using the previously generated spectral library, and the following parameters: 20 peptides/protein; 6 fragment ions/peptide; extraction windows of 5 min and 25 ppm; peptide FDR of 1% and confidence score threshold of 95%. Normalisation of the protein abundance signal as measured by SWATH was carried out using MarkerView (v1.2.1, Sciex).

RNA Isolation and qPCR analysis

Total RNA was isolated from WAT using the RNe-asy Mini Kit (Qiagen), according to the manufacturer's instructions. Complementary DNA (cDNA) (0.5 μ g of total RNA) synthesis and the relative quantification of *TDP-43*, *UCP-1*, *C/EBPβ* and *PPARγ* were performed as described previously [14]. The 18S rRNA was used as a control to normalize gene expression [13]. The reactions were run on an CFX96 Real-Time System instrument and software (CFX Manager 3.0) (BioRad) according to the manufacturer's protocol. Primers were designed using NCBI/Primer-BLAST software (Table 1). Relative quantification for each gene was performed by the $\Delta\Delta$ Ct method [28].

Table 1 List of RT-qPCR primers

Gene	Forward primer	Reverse primer	Acc no	
TDP-43	GGGCGATGGTGACTGTAA	GCTCGTCTGGGCTTTGCTTA	NM_145556	
UCP-1	GGCCTCTACGACTCAGTCCA	TAAGCCGGCTGAGATCTTGT	NM_009463	
C/EBPβ	GACAAGCTGAGCGACGAGT	CGCACCGCGATGTTGTTG	NM_001287738	
PPARy	AGAGGTGGCCATCCGAATTT	ACGGCTTCTACGGATCGAAA	NM_011146	

Primers used for RT-qPCR analysis of the genes assessed here, including the gene symbol, primer sequence (forward and reverse sequence respectively) and GenBank accession number

Protein extraction and western-blot analysis

Proteins from WAT were extracted using RIPA buffer (Sigma Aldrich) containing a cocktail of protease inhibitors (Roche) as described previously [16]. Denatured protein samples (20 µg) from each group were electrophoresed into Bolt® Bis-Tris Plus gels (Invitrogen), transferred to PVDF membranes (BioRad and incubated with rabbit anti-TDP-43 (1:1000; Proteintech) overnight. Subsequently, anti-rabbit horseradish peroxidase (HRP)-conjugated secondary antibody (Vector Laboratories) was used as described previously (https:// doi.org/10.3390/ijms221910305). Mouse (1:1000; Cell Signalling) was used as a loading control and band intensity was measured as the integrated intensity using ImageJ software (v1.4; NIH). All data were normalized to control values on each membrane.

Human plasma samples

All procedures performed in studies involving human samples (plasma) were in accordance with the.

Ethics Committee (783/23/98) of the University CEU-San Pablo, Madrid, Spain. Human plasma samples were provided by the Biobank HUB-ICO-IDIBELL, integrated in the ISCIII Biobanks and Biomodels Platform and they were processed following standard operating procedures with the appropriate approval of the Ethics and Scientific Committees.

Patients were eligible for inclusion if they had diagnosis of ALS based on Gold Coast criteria [39]. Controls were also provided by the Biobank HUB-ICO-IDIBELL. Samples were collected at the hospital using Lithium heparin collecting tubes at the time of diagnosis. Samples were centrifuged at 10,000 RPM for 10 min. The supernatant was collected and frozen at –80 degrees Celsius.

ALS patients were classified by sex, BMI and survival. Patients were classified as nonobese (BMI, < 25) and obese (BMI, \ge 25). BMI was calculated at the time of diagnosis. Patients were classified as slow progressors when survival was higher than 5 years, as normal progressors when survival was between 3 and 5 years, and as fast progressors when survival was less than 3 years. All the human samples included were of patients who were already deceased at the time of the study.

Measurement of plasma leptin by ELISA

ELISAs were performed as suggested by the manufacturer's protocol. Leptin plasma levels were measured using a Human Leptin ELISA Kit PicoKine[®] (Boster Biological Technology) with samples diluted 1:20 for males and 1:10 for females. Each patient's samples were processed in duplicate. The limit of detection was 62.5 pg/mL, and the within-assay and between-assay coefficient of variability (CVs) were 7.8% and 6.5%, respectively.

Statistical analysis

Statistical analyses were performed using Graph-Pad Prism software v10.2.0. Normality of datasets was assessed by Kolmogorov-Smirnov Test. Outliers were removed with ROUT method with Q=1%. For IHC Mann-Whitney test was used. For molecular biology analysis, two-way ANOVA was used followed by Dunett's post hoc test to compare all groups with control WT asymptomatic mice, while Tukey's post hoc test was used for multiple comparisons between all groups. To compare within the same group, t-test test was used. For ELISA, two-way ANOVA was used followed by Tukey's post hoc test for multiple comparisons between all groups. Mann-Whitney test was used to compare within the same group. A Spearman correlation coefficient (rho) was employed to assess the correlation between quantitative variables, with significance set at a p-value of ≤ 0.05 (n=78). This analysis was performed with SPSS Statistics. Values were reported as means ± standard error of the mean (SEM). For all comparisons, significant results were taken when p value < 0.05.

Results

Histological examination of WAT reveals significant alterations in TDP-43^{A315T} mice

Given the limited understanding of how WAT is altered during the progression of ALS, we aimed to address this gap by performing a comprehensive histological characterization of scWAT and pgWAT tissues across the three stages of the disease -asymptomatic ($\sim 42-45$ days (d) of age), onset ($\sim 65-70$ d of age) and end-stage ($\sim 95-100\pm 2$ d of age)- in TDP-43^{A315T} mice, compared to age-matched WT littermates, using H&E staining analysis. We first evaluated CLSs and the number of BV in histological sections (Figs. 1A–C, 2A–C and 3A–C),

(See figure on next page.)

Fig. 1 Hematoxylin and eosin stained scWAT and pgWAT in asymptomatic stage of male TDP-43^{A315T} mice. **A** Representative images of CLSs and BV (section bar = 100 µm). **B** Semi-quantitative analysis of CLSs and **C** BV. **D** Representative images of mononuclear infiltrated, fibrosis and necrosis markers. **E** Semi-quantitative analysis of mononuclear infiltrated, **F** fibrosis, **G** normal membranes shape of AD and **H** integrity of WAT. Abbreviations: scWAT, subcutaneous adipose tissue; pgWAT, perigonadal adipose tissue, CLS, crown-like structures; BV, blood vessels; AD, adipocyte; WAT, white adipose tissue

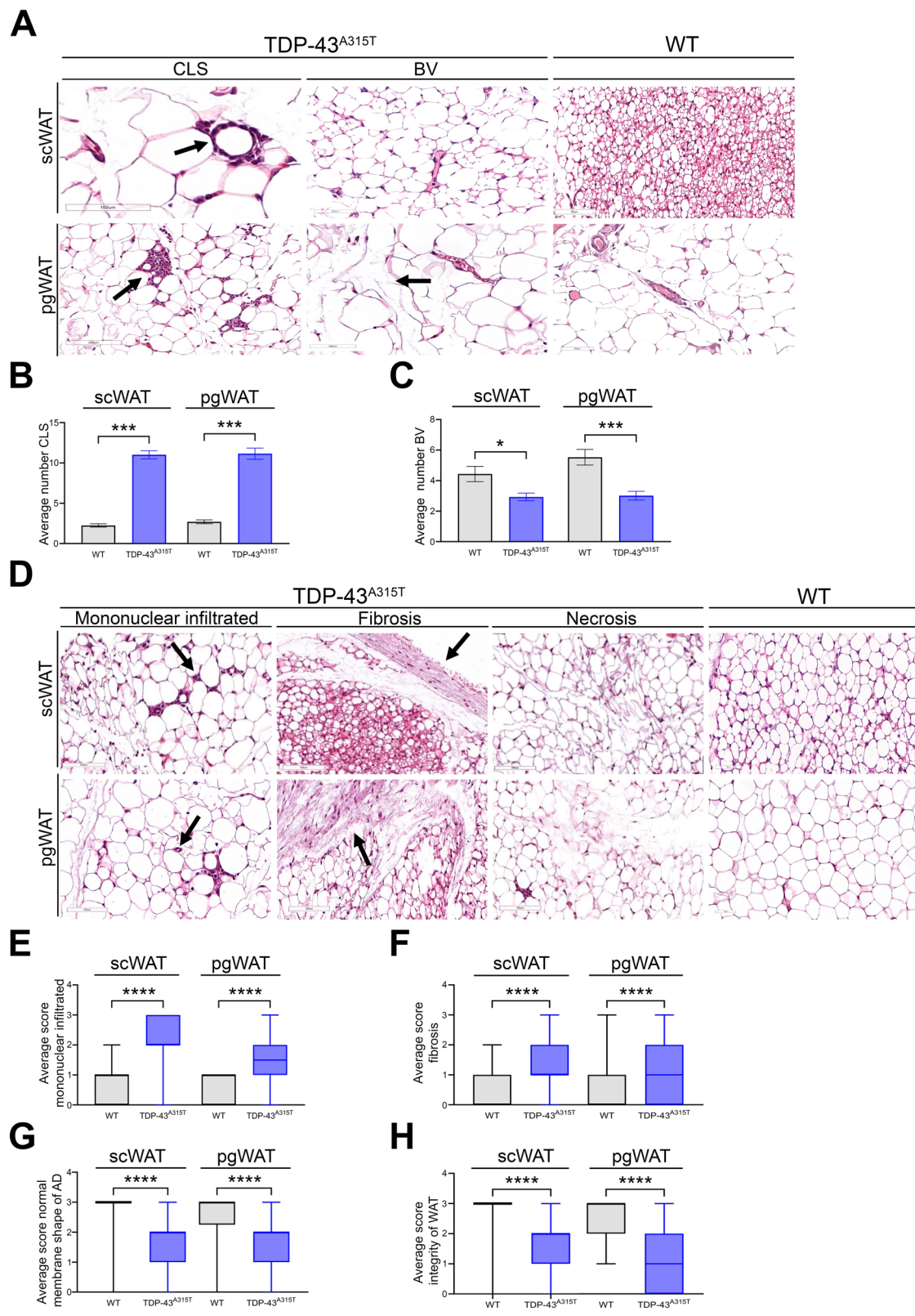


Fig. 1 (See legend on previous page.)

and IHC analysis demonstrated marked differences in the number of both parameters in scWAT and pgWAT, respectively, during the clinical course of the disease in TDP-43^{A315T} mice compared with WT samples (Figs. 1B, C, 2B, C and 3B, C). Mann-Whitney test demonstrated a statistically significant increase in the number of CLSs and BV in both scWAT and pgWAT tissues during the asymptomatic stage in TDP-43A315T mice compared to WT mice (Fig. 1B and C, respectively). The decrease in BV suggests an alteration in the vascularity of the WAT of TDP-43A315T mice (Fig. 1C). However, Mann-Whitney test revealed a statistically significant increase in the number of CLSs in both scWAT and pgWAT tissues at the onset and end-stage of the disease in TDP-43A315T mice (Figs. 2B and 3B, respectively). Additionally, a statistically significant decrease in the number of BV was observed in both scWAT and pgWAT tissues at both disease stages, compared to age-matched WT littermates (Figs. 2C and 3C).

To gain deeper histological insight into the pathological modifications occurring in WAT during the progression of ALS, we further evaluated mononuclear infiltrate, fibrosis and necrosis in both scWAT and pgWAT tissues at the three stages of the disease in TDP-43A315T mice vs. WT samples (Figs. 1D-H, 2D-H and 3D-H). IHC analysis demonstrated a statistically significant increase on inflammatory marker of mononuclear infiltrate at the asymptomatic stage (Fig. 1E) and during the symptomatic and end-stage of the disease (Figs. 2E and 3E, respectively) in TDP-43A315T mice compared to WT mice. Mann-Whitney test demonstrated a statistically significant increase on the fibrosis in both scWAT and pgWAT tissues TDP-43A315T mice compared to WT controls at the three stages of the disease (Figs. 1F, 2F and 3F). Regarding adipocyte shape and tissue integrity there was a significant decrease in both scWAT and pgWAT tissues in TDP-43^{A315T} mice compared to WT mice at the three stages of the disease (Figs. 1G, H, 2G, H and 3G, H).

Proteomics analysis of WAT from TDP-43^{A315T} mice highlighted the presence of mitochondrial alterations prior to the onset of motor symptoms

To further elucidate the molecular alterations occurring in WAT of TDP-43^{A315T} mice, we conducted a proteomic analysis of pgWAT. We focused our analysis on pgWAT,

as in this type of WAT where fibrosis and inflammation are increasingly appreciated as a major player in adipose tissue dysfunction, and pgWAT had substantially higher pro-inflammatory characteristics than scWAT. In this context, using a significant threshold of p < 0.05, proteins having FC > 2 were determined as up-regulated, whereas the ones with FC < 0.5 were down-regulated.

Focusing on the asymptomatic stage of the disease, a total of 1528 proteins were detected as proteins differentially expressed (DEPs) in TDP-43A315T mice compared to age-matched WT littermates. Of these DEPs, 38 showed to be upregulated, 24 downregulated, and 1466 showed no statistically significant differences (Fig. 4A). Enrichment and ontology analyses were performed in Metascape, considering upregulated and downregulated DEPs. Enriched ontology cluster network showed significant enrichment of terms mainly related to two categories: carbon metabolism and monocarboxylic acid metabolic process (Fig. 4B). MCODE clustering analysis recognized 4 different clusters in the protein-protein interaction (PPI) network (Fig. 4C-D; Table 2). MCODE1 represented ontology terms related to mitochondrial fatty acid beta-oxidation and respiratory electron transport. MCODE2 represented ontology terms related with mitochondrial oxidoreductases and ligase and MCODE4 with oxidoreductase and transferases. Though, MCODE3 represents ontology terms related with heme-degradation, scavenging of heme from plasma and lipid-transport. Cellular enrichment analysis showed DEPs grouped together in mitochondria, peroxisome and cytosol (Fig. 4E).

Furthermore, focusing on the end-stage of the disease, 121 DEPs were identified from a total of 1569 proteins in TDP-43^{A315T} mice compared to age-matched WT littermates. Among these DEPs, 75 showed to be upregulated, 46 downregulated and 1448 showed no statistically significant differences (Fig. 5A). Upregulated and downregulated DEPs were considered for the enrichment and ontology analyses performed in Metascape. Enriched ontology cluster network showed significant enrichment of terms mainly related to three categories: cellular catabolic process, terpenoid metabolic process and metabolism of xenobiotics by cytochrome p450 (Fig. 5B). MCODE clustering analysis recognized 2 different clusters in the PPI network (Fig. 5C, D; Table 2). MCODE1

(See figure on next page.)

Fig. 2 Hematoxylin and eosin stained scWAT and pgWAT in onset stage of TDP-43^{A315T} mice. A Representative images of CLSs and BV (section bar = 100 μm). B Semi-quantitative analysis of CLSs and C BV. D Representative images of mononuclear infiltrated, fibrosis and necrosis markers. E Semi-quantitative analysis of mononuclear infiltrated, F fibrosis, G normal membranes shape of AD and H integrity of WAT. Abbreviations: scWAT, subcutaneous adipose tissue; pgWAT, perigonadal adipose tissue, CLS, crown-like structures; BV, blood vessels; AD, adipocyte; WAT, white adipose tissue

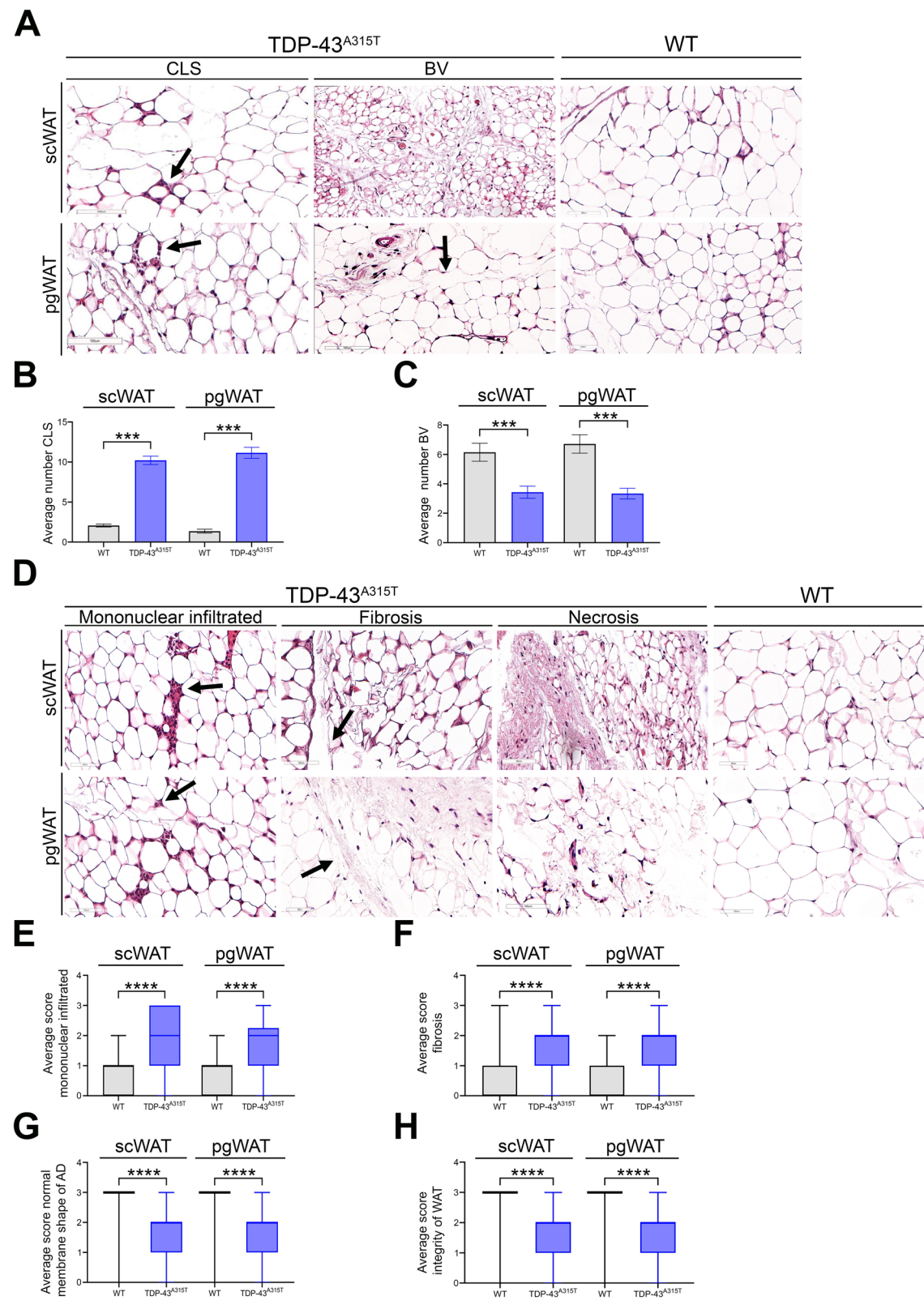


Fig. 2 (See legend on previous page.)

represented ontology terms related to lyases, transferases, oxidoreductases, proteins transport, ribonucleoproteins and RNA and DNA binding. MCODE2 represented ontology terms related to transferases, monooxygenases and oxidoreductase. Cellular enrichment analysis showed DEPs grouped together in cytoplasm, endoplasmic reticulum and mitochondrion, among others (Fig. 5E).

Table 2 reports the list of MCODE cluster recognized by the integrated Metascape analysis of proteomic data showed in Figs. 4C, D and 5C, D. For each cluster, the top 3 enriched terms are reported, relatively to the lowest *p*-value.

WAT of TDP-43. A315T mice display altered *PPARy* mRNA expression levels concomitantly with an increase on the protein levels of TDP-43

Proteomic analysis highlighted several alterations in pgWAT at the asymptomatic stage in TDP-43^{A315T} mice, highlighting the presence of mitochondrial alterations, which could potentially impact both cellular differentiation and metabolism. Thus, to better characterize such defects we performed RT-qPCR in the pgWAT of TDP-43A315T mice over the time course of the disease. RTqPCR analysis demonstrated no statistically significant differences in the mRNA expression levels of C/EBPB and PPARy between TDP-43A315T and WT mice at either of the time-points analysed (Fig. 6A, B). In addition, RTqPCR analysis detected no *Ucp1* mRNA in the pgWAT. We then sought to better characterize the patterns of TDP-43 transgene expression in pgWAT of TDP-43^{A315T} mice compared to age-matched WT littermates. In concordance with the pathological modifications occurring in pgWAT prior to the onset of motor symptoms in TDP-43^{A315T} mice, endogenous TDP-43 mRNA levels (mTDP-43) were significantly upregulated in TDP-43^{A315T} mice compared to WT mice during the asymptomatic stage (p=0.005; Fig. 6C), while no statistically significant differences were found between TDP-43A315T and WT mice at both onset and end-stage. Interestingly, western blot analysis showed that TDP-43 protein levels in pgWAT, probed with a polyclonal antibody that recognizes both human and mouse TDP-43, were increased in TDP-43^{A315T} mice compared to WT mice at either of the timepoints analysed (Fig. 6D-F; Suppl. Figure 1).

Distinct plasma leptin profile in obese men ALS cases with rapidly progressive disease

It is unclear whether changes in WAT precede the first signs of ALS, and whether these alterations are manifested systemically through fluctuations in plasma leptin levels, which are known to be influenced by sex and age. Thus, to better understand the mechanisms regulating WAT disruption and the sexual dimorphism, circulating leptin levels were measured in ALS patients. In total, we measured leptin levels in plasma samples of 62 ALS patients and 16 age-matched controls, with 37 men and 41 women of a wide age (30—87 yr) and BMI (19.06—33.90 kg/m2) range. No statistically significant difference between patients and control groups was found regarding age (p=0.5749) nor BMI (p=0.6940) (Table 3).

ELISA analysis showed that leptin levels in plasma are increased in ALS patients compared to controls, though it is not significant (Fig. 7A). Sorting data by sex, leptin levels were significantly increased in plasma of men ALS patients compared to men controls, as well as in women ALS patients when compared to men ALS patients (Fig. 7B, p=0.009 and p<0.001, respectively), while no statistically significant differences were found in women ALS patients compared to women controls. However, when stratifying patients by sex and survival rate, it is observed that plasmatic leptin levels increased significantly in women ALS patients that have had a normal disease progression when compared to men ALS patients with fast disease progression (Fig. 7C, p = 0.040). Furthermore, leptin levels are significantly increased in women ALS patients with fast progression when compared with men ALS with fast progression (Fig. 7C, p < 0.001). Interestingly, when stratifying patients by sex, survival rate and BMI, for overweight ALS patients, the increase in plasma leptin levels was significant in women ALS patients with normal disease progression when compared to men ALS patients with fast disease progression (Fig. 7D, p=0.006) and to men ALS patients with normal progression (Fig. 7D, p=0.013). In addition, plasma leptin levels of women ALS patients with fast disease progression are significantly increased when compared to men ALS with fast disease progression (Fig. 7D, p=0.011). For overweight women ALS patients, levels decreased in both slow and fast progression when compared to levels in women ALS patients

(See figure on next page.)

Fig. 3 Hematoxylin and eosin stained scWAT and pgWAT in end-stage of TDP^{A315T} mice. A Representative images of CLS and BV (section bar = 100 μm). B Semi-quantitative analysis of CLS and C BV. D Representative images of mononuclear infiltrated, fibrosis and necrosis markers. E Semi-quantitative analysis of mononuclear infiltrated, F fibrosis, G normal membranes shape of AD and H integrity of WAT. Abbreviations: scWAT, subcutaneous adipose tissue; pgWAT, perigonadal adipose tissue, CLS, crown-like structures; BV, blood vessels; AD, adipocyte; WAT, white adipose tissue

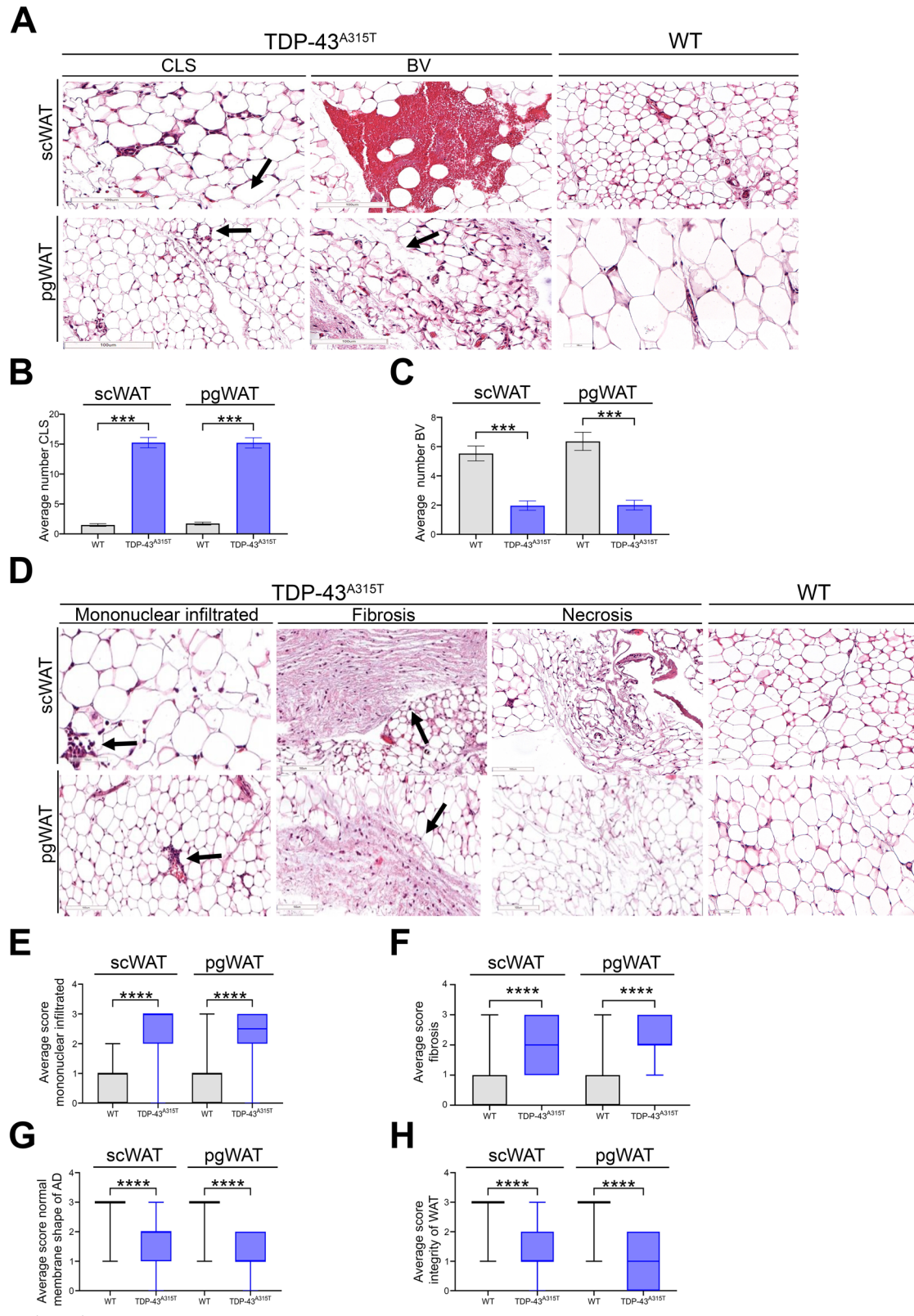


Fig. 3 (See legend on previous page.)

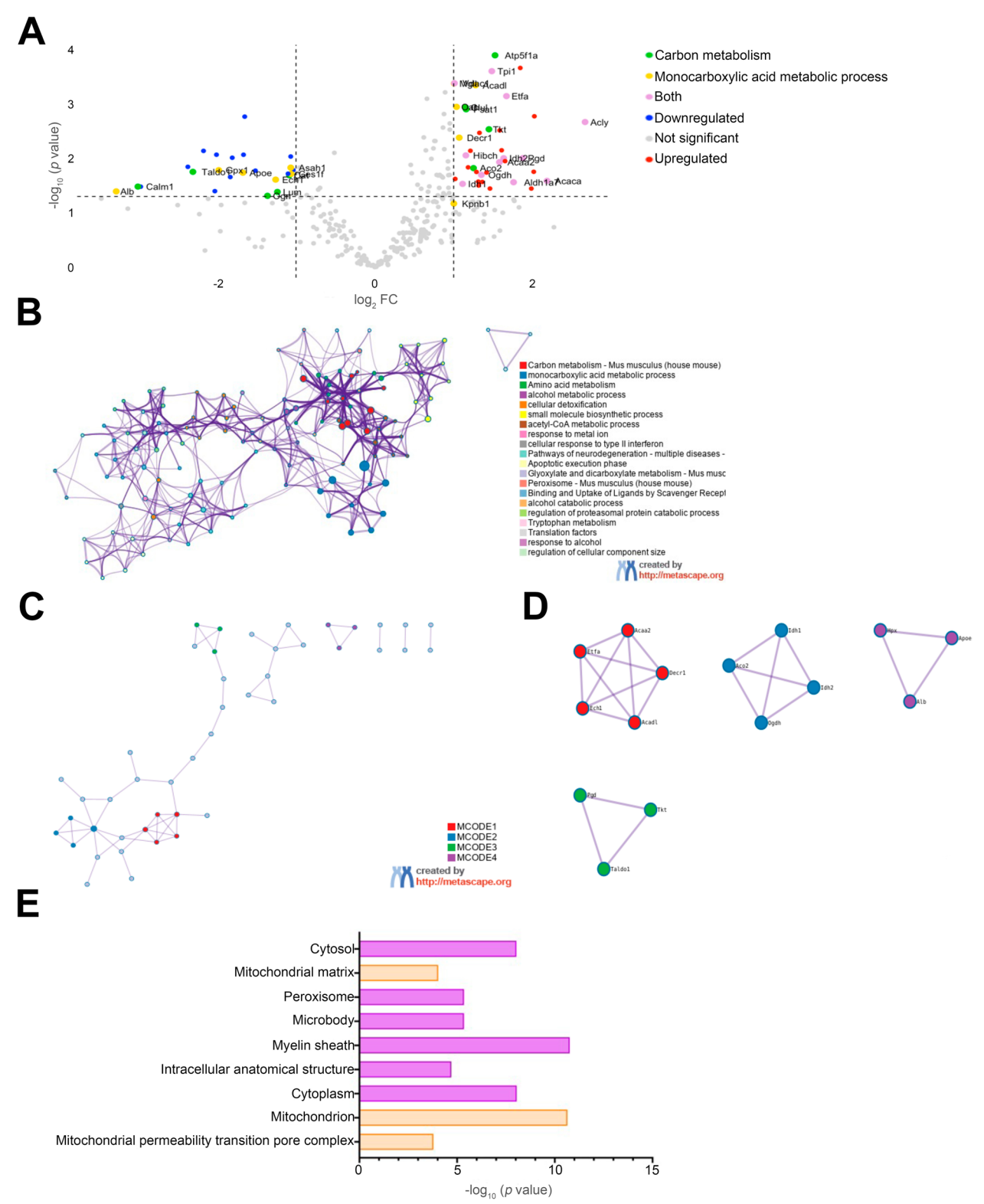


Fig. 4 Proteomic analysis of WAT at asymptomatic stage in TDP-43^{A315T} mice. **A** Volcano plot. Each point represents an individual protein. **B** Enrichment map of representative enriched ontology terms. **C** PPI network colored by MCODE clusters colored by Metascape. **D** PPI network of the separated MCODE clusters from panel C. **E** Cellular component enrichment of DEPs generated with Gene Ontology Software. Abbreviations: WAT, white adipose tissue; PPI, protein–protein interaction; DEPs, proteins differentially expressed

Table 2 MCODE clustering details in asymptomatic and end-stage

	Network	Term ID	Term Description	<i>p</i> -value (-Log10)
Asymptomatic	MCODE_1	GO:0006635	Fatty acid beta-oxidation	
	MCODE_1	GO:0019395	Fatty acid oxidation	-12.0
	MCODE_1	GO:0009062	Fatty acid catabolic process	-11.9
	MCODE_2	Mmu00020	Citrate cycle (TCA cyle)—Mus musculus (house mouse)	-11.4
	MCODE_2	Mmu01210	2-Oxocarboxylyc acid metabolism— <i>Mus musculus</i> (house mouse)	-11.3
	MCODE_2	GO:0006099	Tricarboxylyc acid cycle	-11.3
	MCODE_3	WP63	Pentose phosphate pathway	-10.7
	MCODE_3	GO:0006098	Pentose-phosphate shunt	-9.6
	MCODE_3	R-MMU-71336	Pentose phosphate pathway	-9.5
	MCODE_4	R-MMU-2173782	Binding and Uptake of Ligands by Scavenger Receptors	-8.4
	MCODE_4	R-MMU-5653656	Vesicle-mediated transport	-4.7
End-stage	MCODE_1	GO:0048255	mRNA stabilization	-5.6
	MCODE_1	GO:0043489	RNA stabilization	-5.4
	MCODE_1	GO:1,902,373	Negative regulation of mRNA catabolic process	-5.4
	MCODE_2	Mmu00982	Drug metabolism—cytochrome P450— <i>Mus musculus</i> (house mouse)	-14.9
	MCODE_2	Mmu00980	Metabolism of xenobiotics by cytochrome p450—Mus musculus (house model)	-14.8
	MCODE_2	Mmu05204	Chemical carcinogenesis—DNA adducts—Mus musculus (house mouse)	-14.3

with normal progression, although not significance was reached (Fig. 7D).

Furthermore, bivariate correlations performed are showed in Table 4 and both sex and BMI exhibit a monotonic relationship with leptin levels (p<0.001, r=0.510 and p<0.001, r=0.434, respectively). The correlation of leptin plasma levels with survival rate, as well as the correlation between the qualitative variables, were also evaluated, but no significant differences were found.

Discussion

Although metabolic dysfunctions of the CNS in ALS have been widely studied [37], metabolic alterations observed in ALS patients and animal models have not been well investigated in peripheral organs such as WAT, which play a key role in the endocrine control of energy homeostasis. The current study aimed to better understand whether the WAT plays a critical role in the pathophysiology of ALS, which is of interest as determining how restoring adipose tissue plasticity may contribute significantly to mitigate the hypermetabolism observed in patients with ALS. In this context, we identify for the first time evidence of a pathological dysfunction in WAT prior to the symptomatic stage of the disease in TDP-43^{A315T} mice, providing novel insights about the pathways that could link dysregulating systemic energy homeostasis to the progression of ALS. Additionally, an important finding of our study was that circulating leptin levels at the time of diagnosis were lower in the plasma of overweight and obese men with ALS who exhibited rapid disease progression, emphasizing the importance of considering sex-specific approaches in the development of effective clinical therapies.

Here, we report a significant pathological dysfunction of WAT prior to the symptomatic stage of the disease in TDP-43^{A315T} mice. We observed a significant increase in the number of CLSs in both scWAT and pgWAT adipose tissues, along with a decrease in BV density, suggesting impaired vascularity in WAT prior to the onset of motor symptoms in TDP-43A315T mice. Our results also confirm stage-dependent alterations in inflammatory markers of mononuclear infiltrates. These findings are relevant, as inflamed adipocytes secrete proinflammatory cytokines such as tumor necrosis factor-alpha (TNF α), which disrupt adipose tissue function and limit its expandability. Consistent with previous work in rNLS8 mice [45], we found that the beneficial effects of short-term highfat diet (HFD) therapy in ALS models may not be solely due to weight gain, but rather depend on the capacity of WAT to undergo healthy expansion [36]. Impaired WAT remodeling leads to altered lipid storage and metabolic dysfunction, including dysregulated adipokine production [31]. This supports our earlier findings of significantly reduced peripheral leptin levels from the pre-onset stage in TDP-43A315T mice [16], potentially affecting energy intake regulation. Proteomic analysis of WAT in TDP-43^{A315T} mice revealed significant alterations, including mitochondrial dysfunction, which can alter the cellular homeostasis of WAT and the adipocytes [6], and increased TDP-43 protein levels across disease stages compared to WT littermates. These findings are consistent with previous reports that TDP-43 regulates

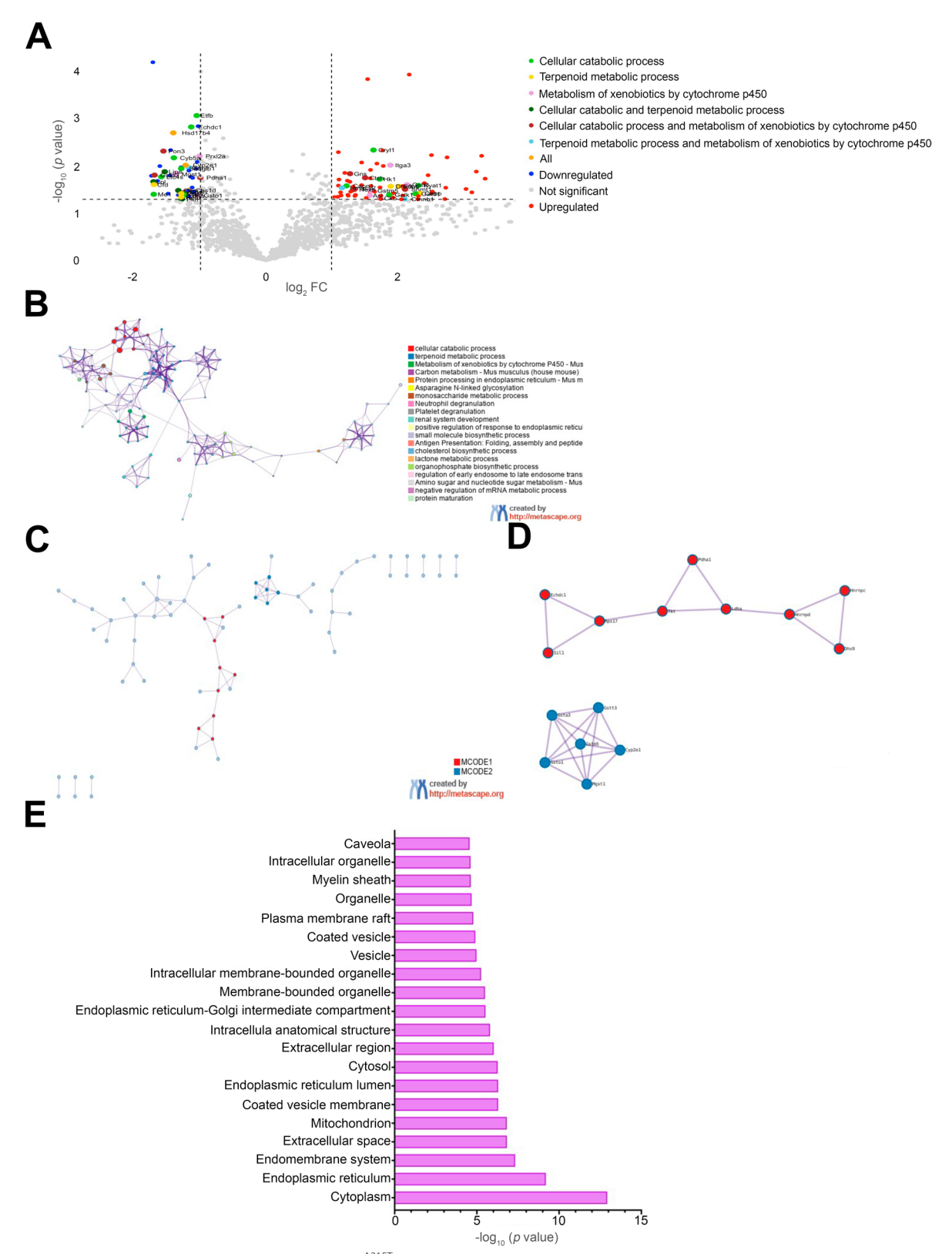


Fig. 5 Proteomic analysis of WAT at end-stage in TDP-43^{A315T} mice. **A** Volcano plot. Each point represents an individual protein. **B** Enrichment map of representative enriched ontology terms. **C** PPI network colored by MCODE clusters colored by Metascape. **D** PPI network of the separated MCODE clusters from panel C. **E** Cellular component enrichment of DEPs generated with Gene Ontology Software. Abbreviations: WAT, white adipose tissue; PPI, protein–protein interaction; DEPs, proteins differentially expressed

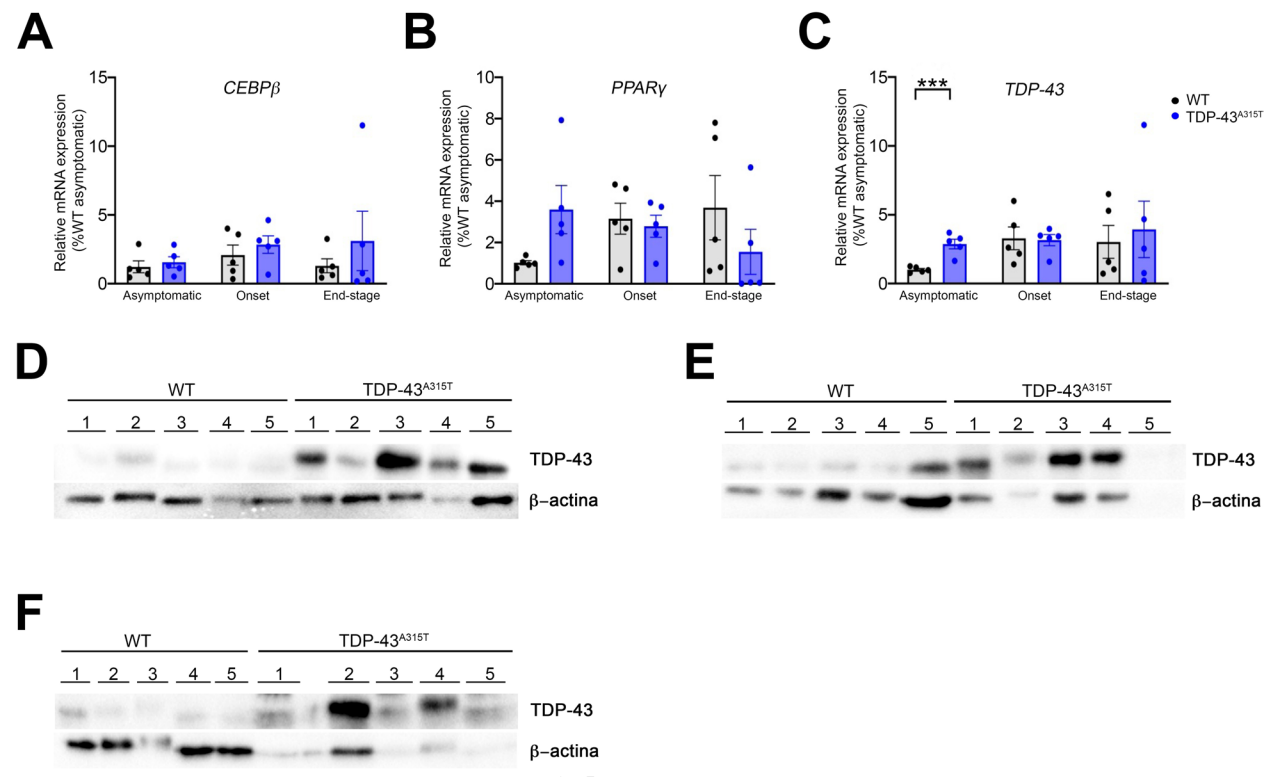


Fig. 6 Alterations in *C/EBPβ*, *PPAR*γ and *TDP-43* in WAT of TDP-43^{A315T} mice. **A** *C/EBPβ* **B** *PPAR*γ and **C** *TDP-43* mRNA expression. Transcripts were assessed by RT-qPCR in TDP-43^{A315T} mice compared to age-matched WT littermates at asymptomatic, onset and end-stage of disease. Values are expressed as the mean \pm SEM for the different groups. TDP-43 protein in WAT extracts of TDP-43^{A315T} mice compared to age-matched WT littermates at asymptomatic **D**, onset **E** and end-stage of disease **F**. *p<0.05, **p<0.01, ***p<0.001, ****p<0.0001. Abbreviations: C/EBPβ, CCAAT Enhancer Binding Protein Beta; PPARγ, Peroxisome proliferator-activated receptor gamma; TDP-43, TAR DNA-binding protein 43; WAT, white adipose tissue; WT, wild-type

body fat composition [42] and may impair leptin signalling through transcriptional regulation [10]. Our data also confirm alterations in leptin signalling in the spinal cord and hypothalamus of TDP-43^{A315T} mice [16], in

Table 3 Characteristics of ALS patients and controls

	ALS	CONTROL
Number of patients	65	16
Age (mean ± SD) (years)	64.27 ± 11.44	65.85 ± 10.93
Sex ratio (male:female)	31:34	7:9
BMI (kg/m ²)	25.99 ± 3.42	25.51 ± 3.75
Disease duration (months)	39.36 ± 18.62	NA
Survival rate slope	1.65 ± 1.04	NA
ALS subtype		
Bulbar	26	NA NA
Espinal	36	
PMA	3	NA
EVOLUTION FORM		
Slow evolution (DPR < 0.8)	8	NA
Normal evolution (0.8 < DPR < 1.35)	23	NA
Fast evolution (DPR > 1.35)	34	NA
Fast evolution (DPR > 1.35)	34	NA

agreement with recent findings in postmortem ALS brain tissue [4].

In patients, altered adipose tissue distribution correlates with functional status and survival [27], and sex differences in endocrine dysfunction have been reported [19]. Our ELISA analysis showed that leptin levels were significantly increased in the plasma of men, but not women, with ALS at diagnosis, compared to controls. However, when stratified by disease progression, leptin levels were significantly lower in overweight men with fast-progressing ALS compared to women. These findings suggest that women may be more protected against ALS, potentially due to hormonal or adipose tissue-related mechanisms.

Although our findings suggest a link between WAT dysfunction and ALS progression, the precise molecular mechanisms remain to be fully elucidated. It is possible that increased TDP-43 levels in WAT impair leptin production and release, contributing to central metabolic dysregulation. However, further experiments are needed to confirm this hypothesis. Sex-related differences in leptin levels and WAT pathology may reflect a

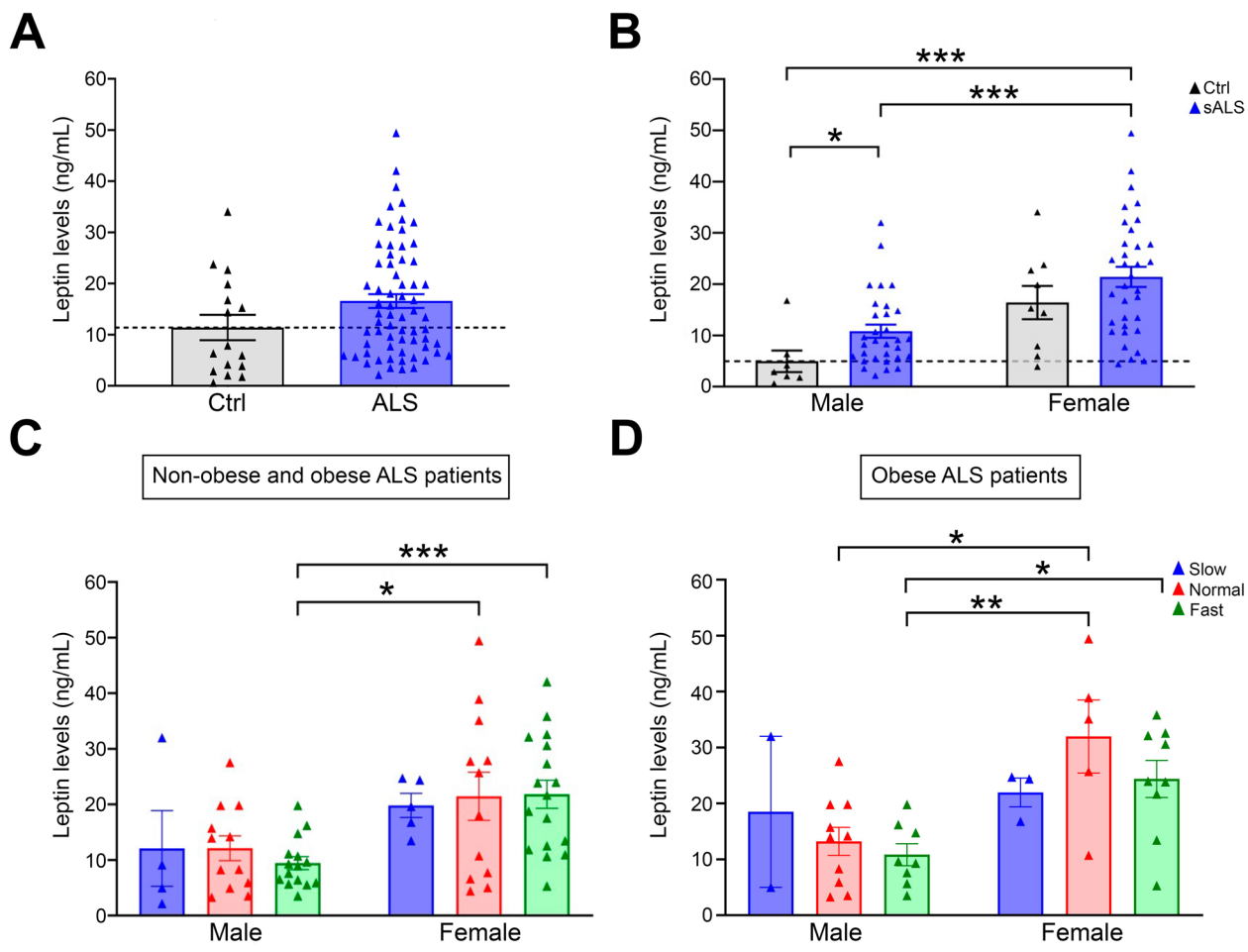


Fig. 7 Analysis of plasma leptin levels in ALS patients. **A** Concentration of leptin levels at diagnosis measured by ELISA in healthy controls and ALS subgrouped by sex. **B** Concentration of leptin levels at diagnosis in ALS and controls subgrouped by sex and disease progression: slow, normal and fast progression patients. **C** Concentration of leptin levels at diagnosis in ALS and controls subgrouped by sex and rate of progression in overweight patients. *p < 0.05, **p < 0.01, ***p < 0.001, ****p < 0.001. Abbreviations: ALS, sporadic amyotrophic lateral sclerosis

Table 4 Spearman correlations

'					
		Leptin	ВМІ	Sex	Survival rate slope
Leptin	r p		0.488 < 0.001	0.488 < 0.001	0.001 0.993
BMI	r p	0.488 < 0.001		-0.027 0.830	-0.063 0.616
Sex	r p	0.488 < 0.001	0.027 0.830		0.005 0.972
Survival rate slope	r p	0.001 0.993	-0.063 0.616	0.005 0.972	

neuroprotective role of female hormones, such as estrogen, particularly in premenopausal women [30]. Alternatively, WAT dysfunction may be less severe in women with ALS. Our unpublished data support this possibility, showing delayed pathological changes in WAT of

female TDP-43^{A315T} mice compared to males, consistent with findings in SOD1^{G93A} mice [34]. These observations highlight WAT as a potential target organ and leptin as a candidate prognostic or diagnostic biomarker in ALS. However, it is important to note that our analysis of plasma leptin levels is cross-sectional, and longitudinal data are currently lacking.

In conclusion, we demonstrate an impairment of WAT during the manifestation of ALS phenotype, which undergoes significant alterations that could potentially impact on the normal physiology of the adipocytes. We showed a significant increase in the number of CLSs, a characteristic histopathology feature of inflamed WAT [32], an alteration in its vascularity, which promotes adipocyte dysfunction and induces oxidative stress, hypoxia and inflammation [3], a stage-dependent alteration on inflammatory marker of mononuclear infiltrate, and significant changes in the proteomic profile, highlighting

mitochondrial alterations, which could significantly disrupt leptin levels [5], during the clinical course of disease in TDP-43^{A315T} mice. These findings suggest that WAT dysfunction may contribute to systemic metabolic imbalance and influence disease progression in ALS.

While these observations provide new insights into the peripheral metabolic disturbances associated with ALS in TDP-43^{A315T} mice, some interpretations remain speculative. For instance, it is possible that the observed WAT alterations reflect developmental defects or secondary responses to neurodegeneration. However, caution is warranted when extrapolating findings from the TDP-43A315T mouse model to clinical settings, as the translational relevance may be limited. Further research in ALS patients is essential to clarify the role of WAT and to better understand the contribution of leptin dysregulation to the metabolic dysfunction associated with pathological TDP-43. Future experimental studies are needed to elucidate the mechanistic links between TDP-43-induced leptin alterations and their impact on functional outcomes and disease-associated molecular phenotypes.

Abbreviations

ACN Acetonitrile AgRP Agoute-related peptide ALS Amyotrophic lateral sclerosis ATP Automatic Tissue Processor BAT Brown adipose tissue **BMI** Body mass index Blood vessels BV cDNA Complementary DNA CLSs Crown-like structures CNS Central nervous system Coefficient of variability CVs

DDA Data-dependent positive ion mode
DEPs Proteins differentially expressed
DPX Dibutyl phthalate xylene

DTT Dithiothreitol

FA Formic acid FTD Frontotempo

Frontotemporal dementia H&F Hematoxvlin and eosin HFD High-fat diet HRP Horseradish peroxidase hTDP-43 Human TDP-43 IAA Iodoacetamide IHC Immunohistochemistry mTDP-43 Endogenous TDP-43 Phosphate buffered saline PBS

pgWAT Perigonadal WAT

POMC Antagonist pro-opiomelanocortin PPI Protein-protein interaction scWAT Subcutaneous WAT SFM Standard error of the mean SP3 Single-pot, solid-phase-enhanced TDP-43 TAR DNA binding protein TNFα Tumor Necrosis Factor alpha **UFMN** Functional Motorneuron Unit

WAT White adipose tissue

WT Wild-type

Supplementary Information

The online version contains supplementary material available at https://doi.org/10.1186/s40478-025-02130-9.

Supplementary file 1.

Acknowledgements

The authors would like to thank the Proteomics Unit of the Hospital Nacional de Parapléjicos for their invaluable technical and analytical assistance in the use of proteomic technology, and the Surgery Unit of the Hospital Nacional de Parapléjicos, Toledo (Spain) for their excellent technical support. In addition, the authors would like to thank patients and Biobank HUB-ICO-IDIBELL (PT20/00171) integrated in the ISCIII Biobanks and Biomodels Platform and Xarxa Banc de Tumors de Catalunya (XBTC) for their collaboration and provide human plasma samples. Finally, Cristina Benito-Casado is supported by a PhD Fellowship from the Consejería de Educación, Ciencia y Universidades Comunidad de Madrid (PIPF-2023/SAL-GL-29613).

Author contributions

C-BC, A-FD collected the tissues; C-BC, E-DM performed histological data analysis; G-BG performed proteomic and provided expertise in data analysis; R-DM, MP provided clinical expertise in data analysis and patient information; C-BC, C-FM performed statistical analysis and prepared the figures. C-FM conceived and designed the study. C-FM drafted the manuscript. All authors critically reviewed the manuscript for intellectual content. All authors have read and agreed to the published version of the manuscript.

Funding

The project leading to these results is funded by "la Caixa" Banking Foundation and co-funded by Fundación Luzón under the project code (LCF/PR/HR19/52160016), Spain.

Availability of data and materials

The datasets used and/or analysed during the current study available from the corresponding author on reasonable request.

Declarations

Ethics approval and consent to participate

All animal procedures were performed in accordance with the Animal Ethics Committee of the Hospital Nacional de Parapléjicos (Approval No 36OH/2019) (Spain) in accordance with the European Communities Council Directive (86/609/EEC) for the Care and Use of Animals for Scientific Purposes. Human samples described in this manuscript were collected under protocols that were reviewed and approved by the Functional Unit of Amyotrophic Lateral Sclerosis (UFELA), Service of Neurology, Bellvitge University Hospital, Hospitalet de Llobregat, (Spain). Subjects underwent informed consent prior to participating in research studies.

Consent for publication

All authors have read and agreed to the published version of the manuscript.

Competing interests

The authors declare no competing interests.

Received: 26 June 2025 Accepted: 15 September 2025 Published online: 09 October 2025

References

 Ahmed RM, Irish M, Piguet O, Halliday GM, Ittner LM, Farooqi S, Hodges JR, Kiernan MC (2016) Amyotrophic lateral sclerosis and frontotemporal

- dementia: distinct and overlapping changes in eating behaviour and metabolism. Lancet Neurol 15(3):332–342. https://doi.org/10.1016/ \$1474-4422(15)00380-4
- Ahmed RM, Phan K, Highton-Williamson E, Strikwerda-Brown C, Caga J, Ramsey E, Zoing M, Devenney E, Kim WS, Hodges JR, Piguet O, Halliday GM, Kiernan MC (2019) Eating peptides: biomarkers of neurodegeneration in amyotrophic lateral sclerosis and frontotemporal dementia. Ann Clin Transl Neurol 6(3):486–495. https://doi.org/10.1002/acn3.721
- AlZaim I, de Rooij LPMH, Sheikh BN, Borgeson E, Kalucka J (2023) The evolving functions of the vasculature in regulating adipose tissue biology in health and obesity. Nat Rev Endocrinol 19(12):691–707. https://doi.org/ 10.1038/s41574-023-00893-6
- Atkinson RAK, Collins JM, Sreedharan J, King AE, Fernandez-Martos CM (2024) Alterations to metabolic hormones in amyotrophic lateral sclerosis and frontotemporal dementia postmortem human tissue. J Neuropathol Exp Neurol 83(11):907–916. https://doi.org/10.1093/jnen/nlae054
- Cavaliere G, Cimmino F, Trinchese G, Catapano A, Petrella L, D'Angelo M, Lucchin L, Mollica MP (2023) From obesity-induced low-grade inflammation to lipotoxicity and mitochondrial dysfunction: altered multi-crosstalk between adipose tissue and metabolically active organs. Antioxidants 12(6):1172. https://doi.org/10.3390/antiox12061172. (Basel, Switzerland)
- Chen W, Zhao H, Li Y (2023) Mitochondrial dynamics in health and disease: mechanisms and potential targets. Signal Transduct Target Ther 8(1):333. https://doi.org/10.1038/s41392-023-01547-9
- Chen-Plotkin AS, Lee VM, Trojanowski JQ (2010) TAR DNA-binding protein 43 in neurodegenerative disease. Nat Rev Neurol 6(4):211–220. https://doi.org/10.1038/nrneurol.2010.18
- Connolly S, Galvin M, Hardiman O (2015) End-of-life management in patients with amyotrophic lateral sclerosis. Lancet Neurol 14(4):435–442. https://doi.org/10.1016/S1474-4422(14)70221-2
- Dardiotis E, Siokas V, Sokratous M, Tsouris Z, Aloizou A, Florou D, Dastamani M, Mentis AA, Brotis AG (2018) Body mass index and survival from amyotrophic lateral sclerosis: a meta-analysis. Neurol Clin Pract 8(5):437–444. https://doi.org/10.1212/CPJ.00000000000000521
- Dokas J, Chadt A, Joost H, Al-Hasani H (2016) Tbc1d1 deletion suppresses obesity in leptin-deficient mice. Int J Obes (2005) 40(8):1242–1249. https://doi.org/10.1038/ijo.2016.45
- Dorst J, Kuhnlein P, Hendrich C, Kassubek J, Sperfeld AD, Ludolph AC (2011) Patients with elevated triglyceride and cholesterol serum levels have a prolonged survival in amyotrophic lateral sclerosis. J Neurol 258(4):613–617. https://doi.org/10.1007/s00415-010-5805-z
- Fayemendy P, Marin B, Labrunie A, Boirie Y, Walrand S, Achamrah N, Coeffier M, Preux P, Lautrette G, Desport J, Couratier P, Jesus P (2021) Hypermetabolism is a reality in amyotrophic lateral sclerosis compared to healthy subjects. J Neurol Sci 420:117257. https://doi.org/10.1016/j.jns. 2020.117257
- Fernandez CM, del Arco A, Gallardo N, Aguado L, Rodriguez M, Ros M, Carrascosa JM, Andres A, Arribas C (2010) S-resistin inhibits adipocyte differentiation and increases TNFalpha expression and secretion in 3T3-L1 cells. Biochem Biophys Acta 1803(10):1131–1141. https://doi.org/10. 1016/i.bbamcr.2010.06.012
- Fernandez CM, Molto E, Gallardo N, del Arco A, Martinez C, Andres A, Ros M, Carrascosa JM, Arribas C (2009) The expression of rat resistin isoforms is differentially regulated in visceral adipose tissues: effects of aging and food restriction. Metabolism 58(2):204–211. https://doi.org/10.1016/j. metabol.2008.09.014
- Ferrer-Donato A, Contreras A, Fernandez P, Fernandez-Martos CM (2022)
 The potential benefit of leptin therapy against amyotrophic lateral sclerosis (ALS). Brain Behav 12(1):e2465. https://doi.org/10.1002/brb3.2465
- Ferrer-Donato A, Contreras A, Frago LM, Chowen JA, Fernandez-Martos CM (2021) Alterations in leptin signaling in amyotrophic lateral sclerosis (ALS). Int J Mol Sci 22(19):10305. https://doi.org/10.3390/ijms221910305
- Goel M, Mittal A, Jain VR, Bharadwaj A, Modi S, Ahuja G, Jain A, Kumar K (2025) Integrative functions of the hypothalamus: linking cognition, emotion and physiology for well-being and adaptability. Ann Neurosci 32(2):128–142. https://doi.org/10.1177/09727531241255492
- Gorges M, Vercruysse P, Muller H, Huppertz H, Rosenbohm A, Nagel G, Weydt P, Petersen A, Ludolph AC, Kassubek J, Dupuis L (2017) Hypothalamic atrophy is related to body mass index and age at onset in amyotrophic lateral sclerosis. J Neurol Neurosurg Psychiatry 88(12):1033–1041. https://doi.org/10.1136/jnnp-2017-315795

- Grassano M, Moglia C, Palumbo F, Koumantakis E, Cugnasco P, Callegaro S, Canosa A, Manera U, Vasta R, De Mattei F, Matteoni E, Fuda G, Salamone P, Marchese G, Casale F, De Marchi F, Mazzini L, Mora G, Calvo A, Chio A (2024) Sex differences in amyotrophic lateral sclerosis survival and progression: a multidimensional analysis. Ann Neurol 96(1):159–169. https:// doi.org/10.1002/ana.26933
- Hatzipetros T, Bogdanik LP, Tassinari VR, Kidd JD, Moreno AJ, Davis C,
 Osborne M, Austin A, Vieira FG, Lutz C, Perrin S (2014) C57BL/6J congenic
 Prp-TDP43A315T mice develop progressive neurodegeneration in the
 myenteric plexus of the colon without exhibiting key features of ALS.
 Brain Res 1584:59–72. https://doi.org/10.1016/j.brainres.2013.10.013
- Heritier A, Janssens J, Adler D, Ferfoglia RI, Genton L (2015) Should patients with ALS gain weight during their follow-up? Nutrition (Burbank, Los Angeles County, Calif) 31(11–12):1368–1371. https://doi.org/10. 1016/j.nut.2015.06.005
- Janse van Mantgem MR, van Eijk RPA, van der Burgh HK, Tan HHG, Westeneng H, van Es MA, Veldink JH, van den Berg LH (2020) Prognostic value of weight loss in patients with amyotrophic lateral sclerosis: a populationbased study. J Neurol Neurosurg Psychiatry 91(8):867–875. https://doi. org/10.1136/jnnp-2020-322909
- Jawaid A, Salamone AR, Strutt AM, Murthy SB, Wheaton M, McDowell EJ, Simpson E, Appel SH, York MK, Schulz PE (2010) ALS disease onset may occur later in patients with pre-morbid diabetes mellitus. Eur J Neurol 17(5):733–739. https://doi.org/10.1111/j.1468-1331.2009.02923.x
- Kershaw EE, Flier JS (2004) Adipose tissue as an endocrine organ. J Clin Endocrinol Metab 89(6):2548–2556. https://doi.org/10.1210/jc.2004-0395
- Lee I, Kazamel M, McPherson T, McAdam J, Bamman M, Amara A, Smith DLJ, King PH (2021) Fat mass loss correlates with faster disease progression in amyotrophic lateral sclerosis patients: exploring the utility of dual-energy x-ray absorptiometry in a prospective study. PLoS ONE 16(5):e0251087. https://doi.org/10.1371/journal.pone.0251087
- Li L, Li B, Li M, Speakman JR (2019) Switching on the furnace: regulation of heat production in brown adipose tissue. Mol Aspects Med 68:60–73. https://doi.org/10.1016/i.mam.2019.07.005
- Lindauer E, Dupuis L, Muller H, Neumann H, Ludolph AC, Kassubek J (2013) Adipose tissue distribution predicts survival in amyotrophic lateral sclerosis. PLoS ONE 8(6):e67783. https://doi.org/10.1371/journal.pone. 0067783
- 28. Livak KJ, Schmittgen TD (2001) Analysis of relative gene expression data using real-time quantitative PCR and the 2(-Delta Delta C(T)) method. Methods (San Diego, Calif) 25(4):402–408. https://doi.org/10.1006/meth. 2001 1262
- 29. Luo L, Liu M (2016) Adipose tissue in control of metabolism. J Endocrinol 231(3):R77–R99. https://doi.org/10.1530/JOE-16-0211
- Manjaly ZR, Scott KM, Abhinav K, Wijesekera L, Ganesalingam J, Goldstein LH, Janssen A, Dougherty A, Willey E, Stanton BR, Turner MR, Ampong M, Sakel M, Orrell RW, Howard R, Shaw CE, Leigh PN, Al-Chalabi A (2010) The sex ratio in amyotrophic lateral sclerosis: a population based study. Amyotrophic Lateral Sclerosis: Official Publication of the World Federation of Neurol Res Group Motor Neuron Diseases 11(5):439–442. https://doi. org/10.3109/1748/961003610853
- Martinez-Sanchez N (2020) There and back again: leptin actions in white adipose tissue. Int J Mol Sci 21(17):6039. https://doi.org/10.3390/ijms2 1176039
- 32. Murano I, Rutkowski JM, Wang QA, Cho Y, Scherer PE, Cinti S (2013) Time course of histomorphological changes in adipose tissue upon acute lipoatrophy. Nutr Metab Cardiovasc Dis 23(8):723–731. https://doi.org/10.1016/j.numecd.2012.03.005
- Ngo ST, Steyn FJ, Huang L, Mantovani S, Pfluger CMM, Woodruff TM, O'Sullivan JD, Henderson RD, McCombe PA (2015) Altered expression of metabolic proteins and adipokines in patients with amyotrophic lateral sclerosis. J Neurol Sci 357(1–2):22–27. https://doi.org/10.1016/j.jns.2015. 06.053
- Picher-Martel V, Boutej H, Vezina A, Cordeau P, Kaneb H, Julien J, Genge A, Dupre N, Kriz J (2023) Distinct plasma immune profile in ALS implicates sTNFR-II in pAMPK/Leptin homeostasis. Int J Mol Sci 24(6):5065. https:// doi.org/10.3390/ijms24065065
- Pico C, Palou M, Pomar CA, Rodriguez AM, Palou A (2022) Leptin as a key regulator of the adipose organ. Rev Endocr Metab Disord 23(1):13–30. https://doi.org/10.1007/s11154-021-09687-5

- Romero-Muñoz L, Sanz-Martos AB, Cabrera-Pinto M, Cano V, Olmo ND, Valiente N, Seseña S, Atkinson RA, Sreedha J, King A, & Fernandez-Martos CM. (2024). Weight gain-mediated recovery of metabolic and gut microbiome impairments in a TDP-43 mouse model of ALS. https://doi.org/10. 21203/rs.3.rs-4015840/v1
- Rosina M, Scaricamazza S, Fenili G, Nesci V, Valle C, Ferri A, Paronetto MP (2025) Hidden players in the metabolic vulnerabilities of amyotrophic lateral sclerosis. Trends Endocrinol Metab. https://doi.org/10.1016/j.tem. 2025 02 004
- Rowland LP, Shneider NA (2001) Amyotrophic lateral sclerosis. N Engl J Med 344(22):1688–1700. https://doi.org/10.1056/NEJM200105313442207
- Shefner JM, Al-Chalabi AAA, Baker MR, Cui L, de Carvalho M, Eisen A, Grosskreutz J, Hardiman O, Henderson R, Matamala JM, Mitsumoto H, Paulus W, Simon N, Swash M, Talbot K, Turner MR, Ugawa Y, van den Berg LH, Verdugo R, Kiernan MC (2020) A proposal for new diagnostic criteria for ALS. Clin Neurophysiol Off J Int Fed Clin Neurophysiol 131(8):1975– 1978. https://doi.org/10.1016/j.clinph.2020.04.005
- Shevchenko A, Wilm M, Vorm O, Mann M (1996) Mass spectrometric sequencing of proteins silver-stained polyacrylamide gels. Anal Chem 68(5):850–858. https://doi.org/10.1021/ac950914h
- Shilov IV, Seymour SL, Patel AA, Loboda A, Tang WH, Keating SP, Hunter CL, Nuwaysir LM, Schaeffer DA (2007) The paragon algorithm, a next generation search engine that uses sequence temperature values and feature probabilities to identify peptides from tandem mass spectra. Mol Cell Proteom MCP 6(9):1638–1655. https://doi.org/10.1074/mcp.T6000 50-MCP200
- 42. Stallings NR, Puttaparthi K, Dowling KJ, Luther CM, Burns DK, Davis K, Elliott JL (2013) TDP-43, an ALS linked protein, regulates fat deposition and glucose homeostasis. PLoS ONE 8(8):e71793. https://doi.org/10.1371/journal.pone.0071793
- Tse NY, Bocchetta M, Todd EG, Devenney EM, Tu S, Caga J, Hodges JR, Halliday GM, Irish M, Kiernan MC, Piguet O, Rohrer JD, Ahmed RM (2023) Distinct hypothalamic involvement in the amyotrophic lateral sclerosisfrontotemporal dementia spectrum. NeuroImageClinical 37:103281. https://doi.org/10.1016/j.nicl.2022.103281
- 44. Vercruysse P, Sinniger J, El Oussini H, Scekic-Zahirovic J, Dieterle S, Dengler R, Meyer T, Zierz S, Kassubek J, Fischer W, Dreyhaupt J, Grehl T, Hermann A, Grosskreutz J, Witting A, Van Den Bosch L, Spreux-Varoquaux O, GERP ALS Study Group, Ludolph AC, Dupuis L (2016) Alterations in the hypothalamic melanocortin pathway in amyotrophic lateral sclerosis. Brain 139(Pt 4):1106–1122. https://doi.org/10.1093/brain/aww004
- Walker AK, Spiller KJ, Ge G, Zheng A, Xu Y, Zhou M, Tripathy K, Kwong LK, Trojanowski JQ, Lee VM (2015) Functional recovery in new mouse models of ALS/FTLD after clearance of pathological cytoplasmic TDP-43. Acta Neuropathol 130(5):643–660. https://doi.org/10.1007/s00401-015-1460-x
- Wegorzewska I, Bell S, Cairns NJ, Miller TM, Baloh RH (2009) TDP-43 mutant transgenic mice develop features of ALS and frontotemporal lobar degeneration. Proc Natl Acad Sci U S A 106(44):18809–18814. https://doi.org/10.1073/pnas.0908767106

Publisher's Note

Springer Nature remains neutral with regard to jurisdictional claims in published maps and institutional affiliations.